Measurement of Gibbs energy of formation of Ca_2PbO_4 using a solid-state cell with three electrodes

K. T. Jacob and K. P. Jayadevan

Materials Research Centre and Department of Metallurgy, Indian Institute of Science, Bangalore 560 012, India

Phase relations in the system Ca–Pb–O at 1100 K have been determined by equilibrating 18 compositions in the ternary and identifying the phases present in quenched samples by X-ray diffraction and energy dispersive X-ray analysis (EDX). Only one ternary compound Ca_2PbO_4 was found to be present. The compound coexists with CaO and PbO. The intermetallic compounds Ca_2Pb, Ca_5Pb_3 and CaPb and liquid alloys are in equilibrium with CaO. The standard Gibbs energies of formation of Ca_2PbO_4 (880–1100 K) and Pb_3O_4 (770–910 K) were determined using solid-state cells based on yttria-stabilized zirconia as the solid electrolyte. Pure oxygen gas at 0.1 MPa was used as the reference electrode. For measurements on Ca_2PbO_4, a novel cell design with three electrodes in series, separated by solid electrolyte membranes, was used to avoid polarization of the electrode containing three solid phases. Two three-phase electrodes were used. The first absorbs the electrochemical flux of oxygen from the reference electrode to the measuring electrode. The other three-phase electrode, which is unaffected by the oxygen flux through the solid electrolyte, is used for electromotive force (EMF) measurement. The results from EMF studies were cross-checked using thermogravimetry (TG) under controlled oxygen partial pressures. The stability of Pb_3O_4 was investigated using a conventional solid-state cell with RuO_2 electrodes. The results can be summarized by the following equations:

$$2CaO + PbO + \tfrac{1}{2}O_2 \rightarrow Ca_2PbO_4 \qquad \Delta_r G^\circ/\mathrm{J\ mol^{-1}} = (-128\,340 + 93.21T/\mathrm{K}) \pm 200$$

$$3PbO + \tfrac{1}{2}O_2 \rightarrow Pb_3O_4 \qquad \Delta_r G^\circ/\mathrm{J\ mol^{-1}} = (-70\,060 + 77.5T/\mathrm{K}) \pm 150$$

As part of systematic studies on phase relations and thermodynamic properties of systems of interest in the area of high T_c oxide superconductors, measurements have been made on the ternary system Ca–Pb–O. In the processing of superconducting phases belonging to the system Bi(Pb)–Sr–Ca–Cu–O, Ca_2PbO_4 is formed in the early stages of the reaction.[1] Phase relations in the system CaO–PbO(PbO_2) in air were explored by Kitaguchi *et al.*[2] using mainly the DTA–TG technique. One interoxide compound, Ca_2PbO_4, having orthorhombic structure[3] and melting incongruently at 1253 ± 2 K was identified. Lead is present in the tetravalent state in this compound. Kuxmann and Fischer[4] have suggested the presence of a hygroscopic compound, Ca_2PbO_3, melting incongruently at 1195 K. The formation of $CaPbO_3$ at high oxygen pressure has also been reported.[5] The phase diagram for the ternary system Ca–Pb–O is not available in the literature. Although Pb_3O_4 is not a stable phase at $T > 920$ K, it can form at lower temperatures. The enthalpy of formation of Ca_2PbO_4 has been measured at 298 K by Idemoto *et al.*[6] using solution calorimetry. A twin heat conduction type calorimeter was used, with a 1.53 M solution of $HClO_4$ as the solvent. The reported enthalpy of formation from elements is -1627.6 ± 0.9 kJ mol^{-1}. Gibbs energies of ternary oxides in the sytem Ca–Pb–O have not been determined. The purpose of this study was to measure phase relations in the ternary and Gibbs energies of formation of interoxide compounds. Solid-state cells, which have been extensively used for accurate thermodynamic measurement on oxides,[7] were selected as the primary tool, supplemented by TG under controlled oxygen partial pressures. A new design of the solid-state cell, with a buffer electrode to absorb the electrochemical flux of oxygen through the solid electrolyte, was used to enhance the accuracy of measurement. For the design of solid-state cells, prior information on phase relations is required.

The low-temperature limit for EMF measurement is increased with the new cell design because of the use of two stabilized zirconia membranes and consequent increase in cell resistance. For studies on the stability of Pb_3O_4 at lower temperatures, a conventional EMF cell with RuO_2 electrodes was used. Catalytic properties of RuO_2 electrodes allow cell response at lower temperatures than possible with Pt electrodes.[8]

Experimental

Materials

Starting materials used in this study had the following nominal purity specifications: Pb, PbO and $CaCO_3$ were 99.99% pure; Ca was 99.9% pure. CaO was prepared by thermal decomposition of $CaCO_3$ in vacuum at 1073 K. The compound Ca_2PbO_4, with light orange colour, was made by pelletizing an intimate mixture of CaO and PbO and heating at 1023 K for 10 h in air. The pellet was crushed and repelletized twice during this period. Attempts to make $CaPbO_3$ by heating an equimolar mixture of CaO and PbO in air were not successful. The product always consisted of a mixture of PbO and Ca_2PbO_4. Attempts were also made to synthesize the compound Ca_2PbO_3 by heating CaO and PbO at 1073 K in evacuated quartz ampoules. The pelletized mixture of oxides was contained in a small zirconia crucible placed inside the quartz ampoule. There was no evidence for the formation of Ca_2PbO_3. The oxide Pb_3O_4 was prepared by oxidizing PbO in oxygen at 800 K. The alloys and intermetallic compounds were prepared by heating the pure metals in the required molar ratios in closed iron crucibles under flowing inert gas. The identification of interoxide compound and intermetallic phases was made by powder X-ray diffraction (XRD). High-purity (99.999%) gases, O_2, Ar and their mixtures, were dried by passage through columns containing silica gel and anhydrous $MgClO_4$. Gas mixtures were made by admitting component gases into a cylinder under controlled pressure. Yttria-stabilized zirconia tubes, containing approximately 8 mol% Y_2O_3, were obtained from Corning Glass.

Phase relations in the system Ca–Pb–O

Phase relations at 1100 K were explored by equilibrating different mixtures of alloys and compounds for *ca.* 100 h,

followed by quenching in chilled Hg and phase identification using optical microscopy, XRD and EDX. Preliminary experiments indicated that *ca.* 60 h were sufficient to attain equilibrium. Further heat treatment did not change the composition of the samples. Mixtures containing a metallic phase were equilibrated in closed iron containers kept under pre-purified inert gas flowing at a rate of *ca.* 5 ml s^{-1}. High-purity Ar gas used was dehydrated by passing through anhydrous $MgClO_4$ and P_2O_5, and deoxidized by passing through Cu turnings at 750 K and Ti granules at 1150 K. Samples containing oxide mixtures were equilibrated either in pure oxygen (0.1 MPa) or in evacuated quartz ampoules. These samples were contained in stabilized-zirconia crucibles. Zirconia crucibles were closed with a lid before sealing in quartz ampoules. To check for the attainment of equilibrium, samples of the same overall composition were prepared using different starting materials. Approach to equilibrium was thus verified from different directions.

EMF measurements using a solid-state cell with three electrodes

The cell design used for high-temperature EMF measurements is shown in Fig. 1. It consisted of three distinct compartments, separated by two impervious yttria-stabilized zirconia tubes, each closed at one end. The cell can be represented schematically as follows:

Measuring Electrode $O_2(P^{\vert}_{O_2})$, Pt	(Y_2O_3) ZrO_2 No flux	Buffer Electrode $O_2(P^{\Vert}_{O_2})$, Pt $P^{\Vert}_{O_2} \approx P^{\vert}_{O_2}$	(Y_2O_3) ZrO_2 $\leftarrow$ O^{2-}	Reference Electrode O_2(0.1 MPa), Pt

(1)

The measuring and reference electrodes were contained inside separate zirconia tubes. When the difference in the chemical potential of oxygen between these electrodes is substantial, there is always a small flux of oxygen through the zirconia electrolyte separating them, even in the absence of physical porosity.[9] The electrochemical permeability is caused by the coupled transport of oxygen ions and electrons (or holes) in the solid electrolyte under the oxygen potential gradient. This flow of oxygen can be stopped only by opposing it with an external dc voltage exactly equivalent to the oxygen chemical potential difference.[10]

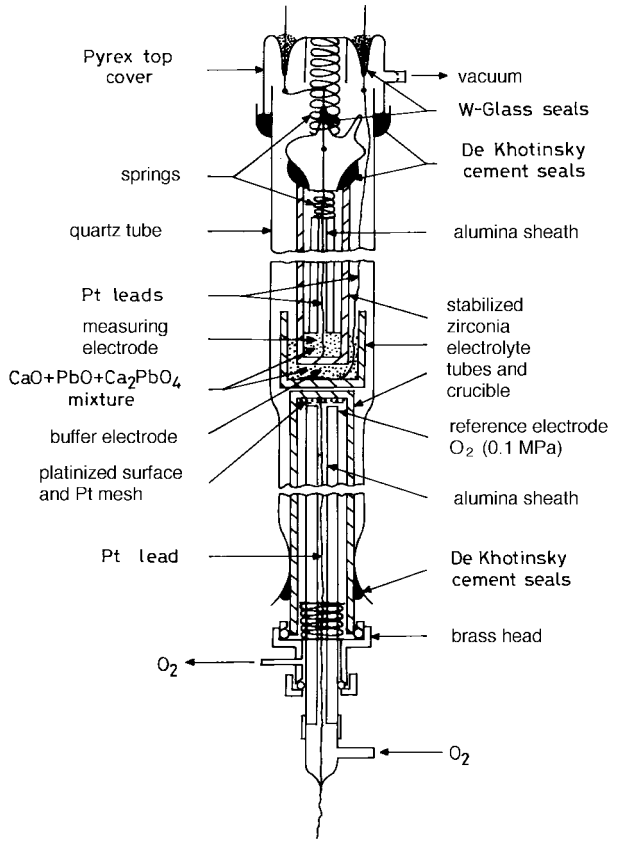

Fig. 1 Schematic diagram of the new apparatus for EMF measurements on Ca_2PbO_4, with a buffer electrode interspaced between measuring and reference electrodes

An electrochemical flux of oxygen would cause polarization of multiphase solid electrodes. The chemical potential of oxygen in the microsystem near the solid electrode/electrolyte interface would be altered because of the semipermeability of the electrolyte to oxygen. The buffer electrode, introduced between reference and measuring electrodes was designed to act as a sink for the oxygen flux and prevent the flux from reaching the measuring electrode. The buffer electrode was maintained at an oxygen chemical potential close to that of the measuring electrode. Since there was no significant difference between the chemical potentials of buffer and measuring electrodes, driving force for transport of oxygen through the zirconia tube separating these electrodes did not exist. The measuring electrode therefore remained unpolarized. Pure oxygen gas at a pressure of 0.1 MPa flowing over a platinized surface of zirconia constituted the primary reference standard for oxygen potential and formed an unpolarizable electrode. Thus, the three-electrode design of the cell prevented error in EMF caused by polarization of the measuring electrode. The magnitude of the polarization effect was assessed by measuring the EMF between the buffer and measuring electrodes.

Construction of the high-temperature galvanic cell was rendered more difficult by the introduction of the buffer electrode. Moreover, in the system under study, the partial pressure of oxygen was quite appreciable, especially at the higher temperatures. Therefore, the static sealed design used by Charette and Flengas[11] was found to be more appropriate than other designs which employ either dynamic vacuum or inert gas flow over the electrodes.[7,12]

The measuring electrode consisted of an intimate mixture of CaO, PbO and Ca_2PbO_4 in the molar ratio of 1:1:1.5. An excess of Ca_2PbO_4 was taken, since some amount of this phase had to decompose initially to establish oxygen pressure in the apparatus. The mixture was rammed against the closed end of a stabilized zirconia tube with a Pt lead embedded in the mixture. An alumina sheath was used to insulate this lead and to press the measuring electrode against the zirconia tube. The top of the zirconia tube was closed with a tight-fitting bell-shaped Pyrex tube, which supported a tungsten electrode connection sealed into the glass. The joint between the bell and the zirconia tube was sealed with De Khotinsky cement. A spring placed between the bell and the alumina sheath applied pressure on the measuring electrode. The assembled measuring electrode half-cell was first evacuated using a side arm tube shown in the diagram, heated to *ca.* 400 K, and then the tube was flame-sealed under vacuum.

The measuring half-cell assembly rested on a buffer electrode contained in a stabilized-zirconia crucible. The buffer also consisted of a mixture of PbO, CaO and Ca_2PbO_4. Thus the partial pressure of oxygen in the buffer was the same as that of the measuring electrode at the start of the experiment. However, in the course of the experiment, the oxygen partial pressure in the buffer increases to a value equivalent to *ca.* 4 mV higher than that of the measuring electrode, because of the oxygen flux from the reference side. The buffer electrode was prepared by consolidating an intimate mixture of constituent phases in the zirconia crucible, with a Pt lead embedded in the powder.

The zirconia crucible rested on another inverted zirconia tube. The mating surfaces of the crucible and tube were polished with diamond paste to minimize resistance. The inside surface of the inverted zirconia tube was platinized. A platinum

gauze was pressed against the closed end of the inverted tube, using an alumina sheath. A Pt lead, spot welded to the gauze, passed through the alumina sheath. The open end of the inverted zirconia tube was fitted with a brass head. Pure oxygen gas at a pressure of 0.1 MPa was flowed through the inverted zirconia tube at a rate of 3 ml s^{-1}. The pressure inside the tube was controlled by a cascade of bubblers placed at the gas exit. The oxygen electrode served as the reference.

The cell was assembled inside a fused quartz enclosure. The inverted zirconia tube containing the reference electrode was first fixed inside the vertical quartz enclosure with De Khotinsky cement. The zirconia crucible containing the buffer electrode was placed on top of the inverted tube. The measuring electrode assembly was then loaded into the crucible. The annular space between the zirconia tube and crucible was filled with the buffer electrode mixture. The measuring electrode assembly was pressed down by means of a second metal spring placed between the bell and the top Pyrex cover. The top cover supported two tungsten-glass seals through which electrical connections were made. All electrode connections were silver soldered. Finally, the top cover was cemented in place by melting the De Khotinsky cement in the ring container shown in the diagram. The cement was allowed to solidify while pressing the top cover against the spring. Then the outer quartz enclosure was also evacuated from a side arm tube and flame-sealed under vacuum. The top half of the cell assembly, shown in Fig. 1, was identical to that developed by Charette and Flengas.[11]

The entire assembly shown in Fig. 1 was placed inside a vertical resistance furnace, with the electrodes located in the even-temperature zone (± 1 K). The upper and lower parts of the assembly, where cement seals were located, remained at room temperature during measurements. A Faraday cage made from the stainless-steel foil was placed between the furnace and the cell assembly. The foil was grounded to minimize induced EMF on cell leads. The temperature of the furnace was controlled to ± 1 K. The temperature was measured by a Pt/Pt–13% Rh themocouple, calibrated against the melting point of gold. The cell potentials were measured with a high-impedance digital voltmeter with a sensitivity of ± 0.01 mV. The potential readings were corrected for small thermal EMFs, measured separately.

Although the cell assembly shown in Fig. 1 consists of three electrode compartments, the cell potential is determined only by the chemical potentials of oxygen in the measuring and reference electrodes. Thus, the effective cell can be concisely written as:

$$\mathrm{Pt, CaO + PbO + Ca_2PbO_4 \| (Y_2O_3)ZrO_2 \| O_2(0.1\ MPa), Pt} \quad (2)$$

The cell is written such that the right hand electrode is positive.

Thermogravimetry

Thermogravimetry of Ca_2PbO_4 was done under controlled oxygen partial pressures. Premixed gases, argon and oxygen, were used to control oxygen partial pressure. The gas mixture from the cylinder was dried by silica gel before use. Gas composition provided by the gas supplier was verified independently using an oxygen gas sensor based on stabilized zirconia. The ratios of oxygen partial pressure to standard pressure in the two gas mixtures used were 1.1×10^{-3} and 2.18×10^{-4}. A commercial TG–DTA apparatus was used to detect decomposition of Ca_2PbO_4. Preliminary experiments at a heating rate of 10 K min^{-1} indicated that at low partial pressures the products of decomposition were solid CaO and PbO. Since at relatively fast heating rates the decomposition temperature might be affected by kinetic factors, further experiments were conducted at a heating rate of 0.5 K min^{-1}. At slow heating rates sharp DTA peaks were not observed. Decomposition temperature was determined from the onset of mass loss of the sample contained in platinum crucibles. On cooling a mass gain was recorded with a hysteresis of *ca.* 8 K, as shown in Table 1. The mean value was taken as the equilibrium decomposition temperature. The decomposition temperatures measured using TG agree well with that calculated from EMF values.

EMF studies on Pb_3O_4

A major disadvantage of the cell design shown in Fig. 1 is its high internal resistance. The design requires two stabilized zirconia membranes between the reference and working electrodes. This restricts the use of such cells to $T > 850$ K. Therefore, a conventional two-electrode design was used for studies on Pb_3O_4. Recently, catalytic electrodes have been developed that permit the measurement of oxygen potential at lower temperature. An electrode made of RuO_2 has been shown to respond to oxygen pressure above 500 K.[8]

A schematic diagram of the apparatus used is shown in Fig. 2. A yttria-stabilized zirconia tube was used as the solid electrolyte. The tube was leak tested and found to be impervious. A coating of RuO_2 was applied on the inside and outside surfaces of the flat closed end of the tube. A 10% aqueous solution of $RuCl_3$ was brushed on to the tube. After drying,

Table 1 Summary of results from thermogravimetry of Ca_2PbO_4

oxygen partial pressure (P_{O_2})/Pa	decomposition temperature on heating/K	reformation temperature on cooling/K	equilibrium temperature/K
111	1058	1050	1054
22.1	1004	996	1000

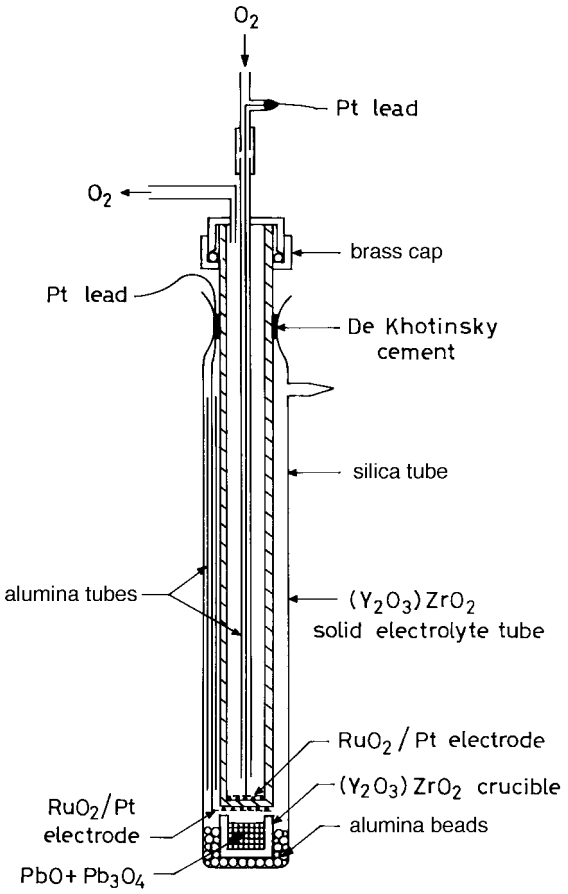

Fig. 2 Schematic diagram of the apparatus used for EMF measurements on Pb_3O_4 at lower temperatures using RuO_2 electrodes

the tube was heated in air at 1073 K for 5 h. A highly adherent black film of RuO_2 was obtained by this treatment. A platinum mesh was placed over the RuO_2 electrode. A platinum wire, wound tightly around the mesh, was used as an electrical lead. Contact with RuO_2 electrode inside the tube was made by pressing a platinum mesh, spot-welded to a platinum wire, against the oxide with an alumina tube.

A mixture of PbO and Pb_3O_4 in the molar ratio 1:1.5 was placed in a zirconia crucible. The solid electrolyte tube was placed over the crucible in such a way as to avoid physical contact between $PbO + Pb_3O_4$ mixture and RuO_2 electrode. The oxygen partial pressure in the gas phase above the $PbO + Pb_3O_4$ mixture was measured by the solid-state cell. The assembly was enclosed in an outer quartz tube. At the cold end, the gap between the neck of the quartz tube and the zirconia tube was closed with De Khotinsky cement as shown in the diagram. After assembling the cell, the quartz tube was evacuated through a side arm to a pressure of 0.1 Pa and then flame sealed. During the experiment, the equilibrium oxygen partial pressure was established inside the quartz tube by the decomposition of Pb_3O_4.

The apparatus was lowered into a vertical resistance furnace and EMF measurements were conducted as described earlier. The cell can be represented as:

$$\mathrm{Pt, RuO_2|PbO + Pb_3O_4\|(Y_2O_3)ZrO_2\|O_2(0.1\ MPa), RuO_2, Pt} \quad (3)$$

Results and discussion

Phase diagram

The isothermal section of equilibrium phase diagram for the system Ca–Pb–O at 1100 K, composed from the results obtained by isothermal equilibration with phase identification by optical microscopy, XRD and EDX, is shown in Fig. 3. Identical phase relations were obtained despite different starting materials used for making samples at a specific composition. Only one oxide PbO was found along the binary Pb–O. PbO can be oxidized in air to Pb_3O_4 at lower temperatures. Along the binary Ca–O, CaO is the only stable phase at 1100 K. Liquid alloys form along two regions on the binary Ca–Pb; $0.015 < X_{Pb} < 0.14$ and $0.575 < X_{Pb} < 1.0$. Three intermetallic compounds, Ca_2Pb, Ca_5Pb_3 and CaPb, were found to be stable. There are seven phase fields in which three condensed phases coexist. All alloys and intermetallic compounds are in equilibrium with CaO.

One ternary oxide, Ca_2PbO_4, was detected in the system. The compound is formed only when a mixture of CaO and PbO is heated in pure O_2 or air. The component binary oxides were found not to react when the mixture was heated in evacuated quartz ampoules. The compound contains Pb in a tetravalent state. The compound Ca_2PbO_4 has an orthorhombic lattice with space group *Pbam* and lattice parameters $a = 0.5839$, $b = 0.9744$ and $c = 0.3379$ nm. It belongs to the Sr_2PbO_4 family. Although this compound has the same space group as Pb_3O_4 below 240 K, there are large differences in lattice parameters. The cell parameters for Pb_3O_4 at 200 K are $a = 0.8818$, $b = 0.8803$ and $c = 0.6562$ nm. At room temperature the space group of Pb_3O_4 is $P4_2/mbc$, with $a = 0.8813$ and $c = 0.6565$ nm. Therefore, significant solid solubility between Pb_3O_4 and Ca_2PbO_4 is unlikely. The phases that coexist with Ca_2PbO_4 at 1100 K are PbO (yellow), CaO and O_2 gas (0.1 MPa). A liquid phase was not observed along the CaO–PbO pseudo-binary at 1100 K. There was no evidence of formation of $CaPbO_3$ or Ca_2PbO_3. The phase diagram suggests that the free energy of formation of Ca_2PbO_4 from CaO and PbO can be obtained by measuring the oxygen partial pressure in the three-phase region.

Gibbs energy of formation of Ca_2PbO_4

The reversible EMF of cell (2) is shown as a function of temperature in Fig. 4. The reversibility of the EMF was established by microcoulometric titration in both directions. A small current (*ca.* 50 μA) was passed through the cell, using an external potential source for *ca.* 5 min and the open-circuit EMF was subsequently monitored as a function of time. The EMF was found to return to the steady value before each titration. During each titration, the chemical potential of oxygen at each electrode was displaced from equilibrium by an essentially infinitesimal amount. Since the electrodes returned to the same potential after such displacements in

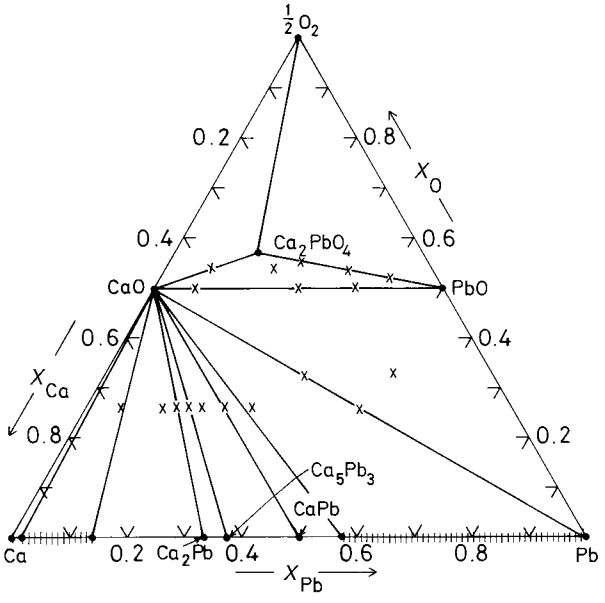

Fig. 3 Isothermal section of the phase diagram for the Ca–Pb–O system at 1100 K. The average bulk composition of samples examined in this study is shown by ×.

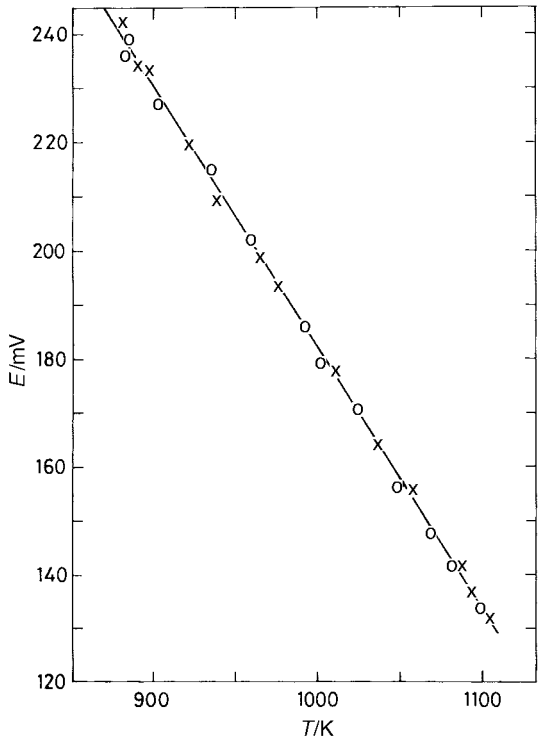

Fig. 4 EMF of cell 2 as a function of temperature. Data from each experiment are shown by the same symbol.

opposite directions, equilibrium was presumed to be attained. The EMF was not affected by the flow rate of oxygen through the reference electrode in the range 2–5 ml s^{-1}. The EMF was also found to be reproducible on temperature cycling in the range 880–1100 K.

With the three-electrode design of the cell, the EMFs were steady (± 0.8 mV) for periods in excess of 10 h. The EMF of the buffer electrode measured against the references was almost identical to that of the measuring electrode at the beginning of the experiments. As a consequence of the flux of oxygen from the reference electrode, the EMF of the buffer electrode against the reference gradually decreased to a value of *ca.* 4 mV lower than that of the measuring electrode by the end of the experiment. This clearly demonstrated the need for the buffer to absorb the oxygen flux and protect the measuring electrode from being disturbed. The EMF of cell (2) is a linear function of temperature, as seen in Fig. 4. The least-squares regression analysis of the EMF gives:

$$E_2/\text{mV} = (665 - 0.483T/\text{K}) \pm 1 \quad (4)$$

The oxygen potential corresponding to the three-phase equilibrium between CaO, PbO and Ca_2PbO_4, and the Gibbs energy of formation of Ca_2PbO_4 from component oxides defined by the equation,

$$2\text{CaO} + \text{PbO} + \tfrac{1}{2}\text{O}_2 \rightarrow \text{Ca}_2\text{PbO}_4 \quad (5)$$

can be obtained directly from the EMF. Since pure CaO, PbO and Ca_2PbO_4 at unit activities are present at the measuring electrode, the standard Gibbs energy change for reaction (5) is related to the relative oxygen chemical potential at the electrode. As pure oxygen at 0.1 MPa is used as the reference electrode, the EMF of cell (2) is directly related to the standard Gibbs energy change for reaction (5),

$$\Delta_{r(5)}G^\circ/\text{J mol}^{-1} = 0.5\Delta\mu_{\text{O}_2} = -2FE_2 = (-128\,340 + 93.21T/\text{K}) \pm 200 \quad (6)$$

where F is the Faraday constant. The yellow form is the reference state for PbO. At 1100 K, the oxygen partial pressure (P_{O_2}/P°) corresponding to the three-phase equilibrium is 3.53×10^{-3}, where P° represents the standard pressure. The temperature-independent term on the right-hand side of eqn. (6) representing the 'second law' enthalpy change for reaction (5) at a mean experimental temperature of 990 K is -128.3 ± 1.5 kJ mol^{-1}. Since the heat capacity of Ca_2PbO_4 has not been measured as a function of temperature, the enthalpy change for reaction (5) at 298.15 K cannot be assessed exactly. However, if the enthalpy change [$\Delta_{r(5)}H^\circ$] is assumed to be independent of temperature, then the standard enthalpy of formation of Ca_2PbO_4 can be estimated by combining the results obtained in this study with standard enthalpies of formation of CaO and PbO.[13] The estimated value for the standard enthalpy of formation from elements at 298.15 K is -1615.8 ± 4 kJ mol^{-1}. The corresponding value obtained by Idemoto *et al.*[6] from solution calorimetry is -1627.6 ± 0.9 kJ mol^{-1}. Part of this difference may be attributed to the change in $\Delta_{r(5)}H^\circ$ with temperature. It would be interesting to measure the low- and high-temperature heat capacities of Ca_2PbO_4 so that a more complete assessment of thermodynamic data for the compound can be performed.

Accurate values for the standard Gibbs energy of formation of PbO_2 are not available at the experimental temperatures to assess the Gibbs energy of formation of Ca_2PbO_4 from constituent oxides CaO and PbO_2. PbO_2 is unstable at these temperatures. An estimate of the standard Gibbs free energy of formation of Ca_2PbO_4 can be obtained from the phase diagram for the system CaO–PbO(PbO_2) in air.[2] The system cannot really be represented as a pseudo-binary. The diagram can at best be considered as a projection of phase relations in the ternary on the pseudo-binary CaO–PbO from the oxygen apex. If seen in this light, a liquid phase rich in PbO, solid PbO and Ca_2PbO_4 are found to coexist at 1120 ± 6 K in air.[2] At 1523 ± 2 K, Ca_2PbO_4 decomposes into a liquid phase containing 85 mol% PbO and solid CaO in air.[2] Assuming Raoult's law behaviour for PbO in the liquid, and using literature data for melting of yellow PbO,[13]

$$\text{PbO(s)} \rightarrow \text{PbO(l)} \quad (7)$$

$$\Delta_{r(7)}G^\circ/\text{J mol}^{-1} = (25\,650 - 12.13T/\text{K}) \pm 200 \quad (8)$$

the standard Gibbs energy of formation of Ca_2PbO_4 at 1253 K can be estimated as $-11\,780 \pm 500$ J mol^{-1}. This estimated value is in good agreement with that obtained from the EMF [$-11\,550 \pm 200$ J mol^{-1}].

Stability of Pb_3O_4

The reversible EMF of cell (3) is displayed as a function of temperature in Fig. 5. The EMF is zero at 904 ± 1 K. This represents the temperature for decomposition of Pb_3O_4 in pure oxygen at 0.1 MPa. The decomposition temperature in air is 834 ± 1 K. Within experimental uncertainty, EMF is a linear function of temperature. Least-mean squares regression analysis yields:

$$E_3/\text{mV} = (363.0 + 0.4016T/\text{K}) \pm 0.8 \quad (9)$$

The standard Gibbs energy of formation of Pb_3O_4 from PbO and O_2 can be obtained directly from the EMF. For the reaction,

$$3\text{PbO} + \tfrac{1}{2}\text{O}_2 \rightarrow \text{Pb}_3\text{O}_4 \quad (10)$$

$$\Delta_{r(10)}G^\circ/\text{J mol}^{-1} = -2FE_3 = (-70\,060 + 77.5T/\text{K}) \pm 150 \quad (11)$$

By combining this result with the standard free energy of formation of PbO reported by Jacob and Jeffes[14] in the temperature range 750 to 1130 K;

$$\text{Pb} + \tfrac{1}{2}\text{O}_2 \rightarrow \text{PbO} \quad (12)$$

$$\Delta_f G^\circ/\text{J mol}^{-1} = (-218\,100 + 98.89T/\text{K}) \pm 420 \quad (13)$$

the standard free energy of formation of Pb_3O_4 from elements

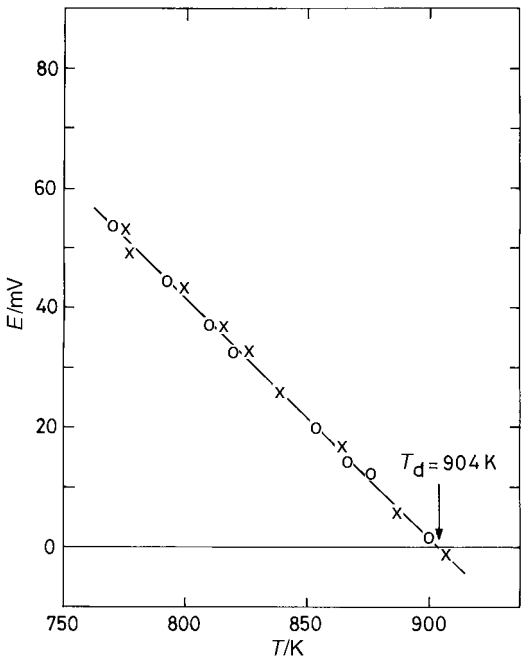

Fig. 5 Variation of the EMF of cell 3 with temperature. Data from each experiment are shown by the same symbol.

can be derived. For the reaction,

$$3Pb + 2O_2 \rightarrow Pb_3O_4 \quad (14)$$

$$\Delta_f G^\circ/\text{J mol}^{-1} = (-724\,360 + 374.17T/\text{K}) \pm 450 \quad (15)$$

in the temperature range 770–910 K. An accurate method for deriving the enthalpy of formation of Pb_3O_4 at 298.15 K is the 'third-law' treatment in which the calorimetric heat capacities and standard entropies of reactants and products are combined with the Gibbs energy data at a specific temperature:

$$\Delta_f H^\circ_{298.15} = \Delta_f G^\circ(T) - \Delta_f(H^\circ_T - H^\circ_{298.15}) + T[\Delta_f S^\circ_{298.15} + \Delta_f(S^\circ_T - S^\circ_{298})] \quad (16)$$

where $\Delta_f(H^\circ_T - H^\circ_{298.15})$ and $\Delta_f(S^\circ_T - S^\circ_{298})$ are the difference in enthalpy and entropy increment, respectively, between products and reactants. If Gibbs energy and thermal data are accurate, then the derived value of $\Delta_f H^\circ_{298.15}$ should be independent of the temperature of Gibbs energy measurement. Drift in $\Delta_f H^\circ_{298.15}$ with temperature is indicative of either temperature-dependent systematic errors in the free energy measurement or inaccurate thermal functions and standard entropies. The 'third-law' analysis gives $\Delta_f H^\circ$ for Pb_3O_4 at 298.15 K as -735.5 ± 0.5 kJ mol^{-1}, using thermal functions for Pb, O_2 and Pb_3O_4 from Pankratz.[13] If thermal functions for reactants and products in the formation reaction (14) are taken from the compilation of Knacke *et al.*,[15] $\Delta_f H^\circ_{298.15}$ for Pb_3O_4 calculated by the 'third-law' method becomes -730.83 ± 0.1 kJ mol^{-1}. Thus there is considerable uncertainty in the values for standard entropy and heat capacity of Pb_3O_4. The drift in $\Delta_f H^\circ_{298.15}$ is less when auxiliary data from Knacke *et al.* are used. The value $\Delta_f H^\circ_{298.15}$ obtained in this study is more negative than the value of -718.69 kJ mol^{-1} given in the compilation of Pankratz,[13] but is in reasonable agreement with the value of -730.67 kJ mol^{-1} given in the tables of Knacke *et al.*[15]

Computation of phase diagrams

The oxygen potential diagram for the system Ca–Pb–O at 1100 K, composed from the results of this study and data from the literature[13] on binary oxides is shown in Fig. 6. The composition of the phases is represented by the cationic fraction, $\eta_{Pb}/(\eta_{Ca}+\eta_{Pb})$, where η_i represents moles of component *i*. Since oxygen is not included in the composition parameter, information on oxygen non-stoichiometry cannot be displayed on the diagram. Nevertheless, the diagram provides useful information on the oxygen potential range for the stability of various phases. The diagram is complimentary to the conventional Gibbs triangle representation of phase relations in ternary systems, where phase composition can be unambiguously displayed. All the topological rules of construction for conventional temperature–composition phase diagrams are applicable to the oxygen potential diagram shown in Fig. 6.

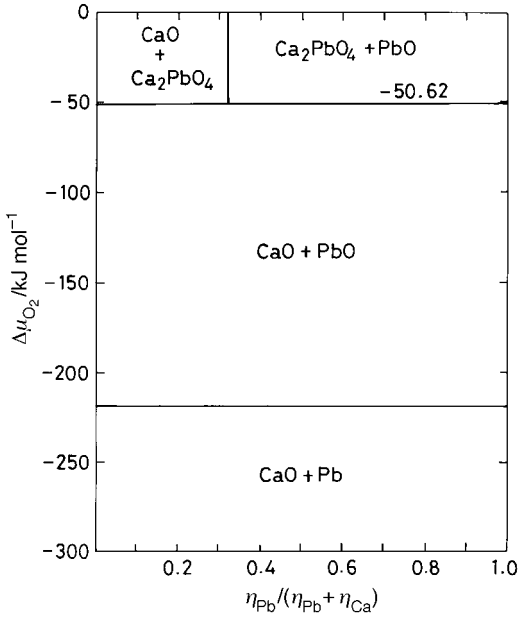

Fig. 6 Oxygen chemical potential diagram for the Ca–Pb–O system at 1100 K

When three condensed phases and a gas phase coexist at equilibrium in a ternary system such as Ca–Pb–O, the system is monovariant; at a fixed temperature, three condensed phases coexist only at a unique partial pressure of oxygen. The three-phase equilibria are therefore represented by horizontal lines on the diagram. The phase equilibria at very low oxygen potentials between alloys and intermetallic compounds on the one hand, and CaO on the other, are not shown on Fig. 6, since activity data for the metallic phases required for the calculation are not available. The oxygen potentials are too low to be measured by currently available techniques. Similar diagrams at other temperatures can be readily computed from the thermodynamic data.

Phase diagrams at constant oxygen partial pressure

Phase relations can also be computed from thermodynamic data as a function of temperature at constant oxygen partial pressures. The computed phase diagrams in air ($P_{O_2} = 2.13 \times 10^4$ Pa) and an oxygen partial pressure of 10.13 Pa are shown in Fig. 7. The decomposition temperature for PbO_2 was calculated from thermodynamic data for the reaction

$$Pb_3O_4 + O_2 \rightarrow 3PbO_2 \quad (17)$$

$$\Delta_{r(17)} G^\circ/\text{J mol}^{-1} = (-120\,530 + 202.25T/\text{K}) \quad (18)$$

The decomposition temperature of Ca_2PbO_4 is considerably higher than that for Pb_3O_4 or PbO_2 at all partial pressures of oxygen. Because of strong binding between the component oxides CaO and PbO_2 in the ternary oxide Ca_2PbO_4, the activity of PbO_2 in the compound is substantially lowered. The strong interaction between CaO and PbO_2 accounts for the high decomposition temperature of Ca_2PbO_4. Fig. 7 shows that the temperature–composition diagram is very sensitive to oxygen partial pressure in the ambient atmosphere.

Since information on oxygen stoichiometry cannot be shown in two-dimensional representation of ternary phase equilibria at constant oxygen partial pressure, a schematic three-

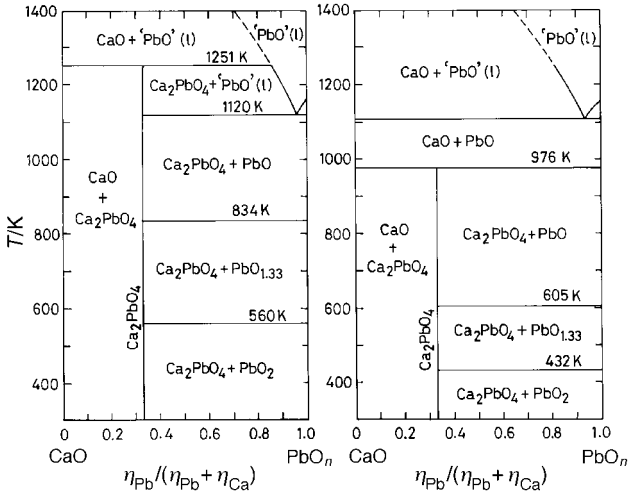

Fig. 7 Phase diagram for the Ca–Pb–O system at fixed oxygen partial pressures: (left) air ($P_{O_2} = 2.13 \times 10^4$ Pa), (right) $P_{O_2} = 10.13$ Pa(10^{-4} atm)

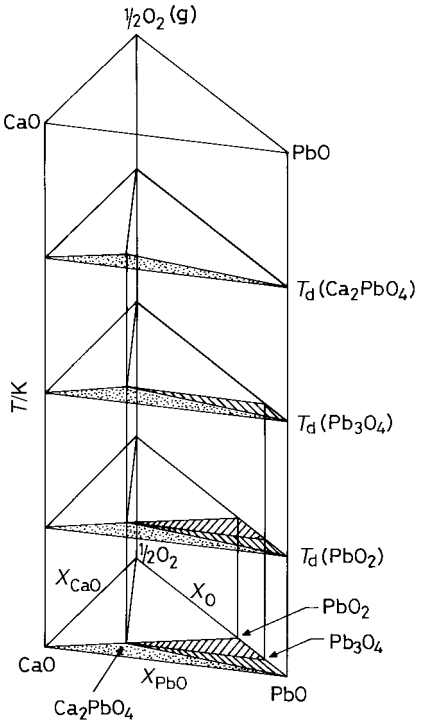

Fig. 8 Schematic subsolidus composition–temperature phase diagram for the ternary CaO–PbO–O system

dimensional sketch of subsolidus phase relations in the subsystem CaO–PbO–O is presented in Fig. 8. Below the decomposition temperature of Pb_3O_4, an additional three-phase region ($PbO + Pb_3O_4 + Ca_2PbO_4$) is generated. Further, below the decomposition temperature of PbO_2, yet another three-phase region ($Pb_3O_4 + PbO_2 + Ca_2PbO_4$) is obtained. The ternary oxide Ca_2PbO_4 can exist in equilibrium with all three oxides of lead, PbO, Pb_3O_4 and PbO_2. Each three-phase region is associated with a unique oxygen partial pressure at constant temperature. As one proceeds from a specific alloy composition towards the oxygen apex along a path of constant ratio η_{Ca}/η_{Pb} on an isothermal section of the phase diagram, phase fields with increasing oxygen partial pressure are encountered.

Conclusion

An experimentally validated ternary equilibrium phase diagram has been constructed for the system Ca–Pb–O at 1100 K. In this system, there exists only one ternary oxide, Ca_2PbO_4. It is stable in pure oxygen, but decomposes to CaO and PbO when oxygen partial pressure is reduced below a critical value. A solid-state cell based on yttria-stabilized zirconia is used to measure the oxygen potential corresponding to three-phase equilibrium involving Ca_2PbO_4, PbO and CaO.There is negligible solid solubility between these oxides. Hence, the standard Gibbs energy of formation of Ca_2PbO_4 is derived from the EMF of the cell. An advanced design of the galvanic cell with a buffer electrode is used to prevent polarization of the three-phase electrode. The results from electrochemical measurements are confirmed by TG at controlled oxygen partial pressures. Use of a RuO_2 electrode on a $(Y_2O_3)ZrO_2$ solid electrolyte permitted precise measurement of the Gibbs energy of formation of Pb_3O_4 at lower temperatures (770 K) than is possible with Pt electrodes. Thermodynamic data were used for deriving an oxygen potential diagram for the system Ca–Pb–O at 1100 K and phase relations as a function of temperature at constant oxygen partial pressures. The data can also be used for computation of phase relations in higher order systems.

References

1 A. Braileanu, M. Zaharescu, D. Crisan and E. Segal, *Thermochim. Acta*, 1995, **269/270**, 553.
2 H. Kitaguchi, J. Takada, K. Oda and Y. Miura, *J. Mater. Res.*, 1990, **5**, 929.
3 M. Tromel, *Z. Anorg. Allg. Chem.*, 1969, **371**, 237.
4 U. Kuxmann and P. Fischer, *Erzmetall.*, 1974, **27**, 533.
5 C. Levy-Clement, I. Morgenstern-Badarau and A. Michel, *Mater. Res. Bull.*, 1972, **7**, 35.
6 Y. Idemoto, K. Shizuka and K. Fueki, *Physica C*, 1994, **255**, 127.
7 J. N. Pratt, *Metall. Trans. A,* 1990, **21**, 1223.
8 G. Periaswami, S. V. Varamban, S. R. Babu and C. K. Mathews, *Solid State Ionics*, 1988, **26**, 311.
9 J. Fouletier, P. Fabry and M. Kleitz, *J. Electrochem. Soc.*, 1976, **123**, 204.
10 K. T. Jacob and J. H. E. Jeffes, *Trans. Inst. Min. Metall., Sect. C*, 1971, **80**, C181.
11 G. G. Charette and S. N. Flengas, *J. Electrochem. Soc.*, 1968, **115**, 796.
12 G. M. Kale and K. T. Jacob, *Metall. Trans. B*, 1992, **23**, 57.
13 L. B. Pankratz, *Thermodynamic Properties of Elements and Oxides, US Bureau of Mines Bull. 672*, US Government Printing Office, Washington, DC, 1982.
14 K. T. Jacob and J. H. E. Jeffes, *Trans. Inst. Min. Metall., Sect. C*, 1971, **80**, C32.
15 O. Knacke, O. Kubaschewski and K. Hesselmann, *Thermochemical Properties of Inorganic Substances*, Springer-Verlag, Berlin, 2nd edn., 1991, vol. II.

Paper 7/05512I; *Received* 29*th July*, 1997